Ceramics International xxx (xxxx) xxx

Contents lists available at ScienceDirect

Ceramics International

journal homepage: www.elsevier.com/locate/ceramint

Crystallographic characteristics and microwave dielectric properties of Ni-modified $MgTa_2O_6$ ceramics

Liang Shi [a,**], Xueying Wang [a], Rui Peng [a], Gang Wang [a], Cheng Liu [a,b], Xiaolei Shi [a], Dainan Zhang [a,b], Huaiwu Zhang [a,b,*]

[a] School of Electronic Science and Engineering, University of Electronic Science and Technology of China, Chengdu, 610054, China
[b] State Key Laboratory of Electronic Thin Films and Integrated Devices, University of Electronic Science and Technology of China, Chengdu, 610054, China

ARTICLE INFO

Keywords:
$MgTa_2O_6$ ceramics
Microwave dielectric
PVL theory
Crystal structure

ABSTRACT

Ni^{2+} modified $MgTa_2O_6$ ceramics with a trirutile phase and space group $P4_2/mnm$ were obtained. The correlations between crystallographic characteristics and microwave dielectric performance of $MgTa_2O_6$ ceramics were systematically studied based on the chemistry bond theory (PVL theory) for the first time. The results indicate that the introduction of Ni^{2+} causes a change in polarizability and the Mg–O bond ionicity, which contributes to the variation of dielectric constant. Moreover, the lattice energy, and packing fraction, full width at half maximum of the Raman peak of Ta–O bond, as the quantitative characterization of crystallographic parameters, regulate the dielectric loss of $MgTa_2O_6$ ceramics in GHz frequency band. In addition, the study of sintering behavior shows that the densification and micromorphology are the crucial factors affecting the microwave dielectric performance. Typically, Ni^{2+} doping on the A-site of $MgTa_2O_6$ can effectively promote the Q × f values to 173,000 GHz (at 7.43 GHz), which ensures its applicability in 5G communication technology.

1. Introduction

In recent decades, Microwave dielectric ceramics (MWDCs) have been widely used in passive devices, such as filters, resonators, dielectric substrates, antennas, etc., owing to their board dielectric spectra, low loss in microwave frequency bands, and good thermal stability. The vigorous development and the extensive commercial application of modern communication technology, such as the Internet of things and 5G, puts forward higher challenges of the base material in a higher operating frequency band [1–5]. However, heat generation of the device is evident at high operating frequencies. Therefore, ensuring lower thermal effect of passive devices at high operating frequencies for modern communication technology applications is an important research topic [6].

It is well known that the size of passive devices is inversely related to the dielectric constant of the substrate. Therefore, to meet the miniaturization requirements of modern communication technology, materials with medium permittivity and low loss are of great concerned. Silicates, molybdates and vanadates have received widely attention for their good microwave dielectric properties. However, silicates with low dielectric constant ($\varepsilon_r < 10$), such as Mg_2SiO_4 [7], Zn_2SiO_4 [8], $SrY_2Si_3O_{10}$, $BaY_2Si_3O_{10}$ [9] ceramics, are not conducive to the miniaturization of the device. Molybdate and Vanadate have high dielectric constants, such as, $BiVO_4$ [10], (Bi, Ce)VO_4 [11], $Bi(Sc_{1/3}Mo_{2/3})O_4$ [12] ceramics, but its dielectric loss is relatively high at GHz frequency band. Typically, the Ta-, Ge- and Nb-containing materials are an essential part of medium dielectric materials. This includes AB_2O_6 (A = Ca, Mg, Mn, Co, Ni, Zn, and B═Nb, Ta) system, which has excellent microwave dielectric properties have attracted public attention [13]. Among the ceramics in this system, the trirutile $MgTa_2O_6$ ceramics with an ε_r of 28 and a Q × f value of 60000 GHz are excellent candidates for miniaturization and high-frequency modern communication technology [14–16]. To improve the practicability of $MgTa_2O_6$ at higher operating frequency, reducing its dielectric loss to control the thermal effect is fundamental. Dang et al. synthesized the Mg-rich Mg–Ta binary system, such as $2MgO–Ta_2O_5$ with an ε_r of 28 and a Q × f value of 211000 GHz [14]. Nb^{5+} to substitute B-site Ta^{5+} of $MgTa_2O_6$ and $ZnTa_2O_6$ to effectively adjust the τ_f value on the premise of sacrificing quality factors (Q × f = 60000 GHz) [17,18]. Equivalent cations (such as Ni^{2+}, Zn^{2+}, and Cu^{2+}) were used to replace the A site of $MgNb_2O_6$ and $Mg_3Nb_2O_8$,

* Corresponding author. School of Electronic Science and Engineering, University of Electronic Science and Technology of China, Chengdu, 610054, China.
** Corresponding author.
E-mail addresses: shiliang_uestc@163.com (L. Shi), hwzhang@uestc.edu.cn (H. Zhang).

https://doi.org/10.1016/j.ceramint.2021.04.260
Received 7 March 2021; Received in revised form 8 April 2021; Accepted 27 April 2021
Available online 30 April 2021

effectively improving their microwave dielectric properties [19,20]. In conclusion, ion introducing into Ta site of $MgTa_2O_6$ ceramics could enhance the microwave dielectric performance. However, there are few explanations about the effect of crystallographic characteristics and microwave dielectric properties caused by Mg-site doping.

Considering the similarity of the ionic radius (R_{Mg} = 0.72 Å, R_{Ni} = 0.69 Å), Ni^{2+} might replace Mg^{2+} to form a pure trirutile-structure. In this work, trirutile-type $Mg_{(1-x)}Ni_xTa_2O_6$ (x = 0.00–0.08) was synthesized. The impact of Ni^{2+} on micro morphology, crystallographic structure, crystal stability, and the dielectric performance of $Mg_{(1-x)}Ni_xTa_2O_6$ ceramics are systematically investigated.

2. Experiment

High-purity MgO, Ta_2O_5 and NiO (all purity>99.9%, Aladdin Industrial Co, Shanghai, China) were weighed based on the stoichiometric ratios of the $Mg_{(1-x)}Ni_xTa_2O_6$ (x = 0, 0.02, 0.04, 0.06, 0.08). The weighed powder was mixed and grind with zirconium ball for 10 h. The mixed oxides were calcined at 1100 °C for 4 h and then pre-formed trirutile phase. Subsequently, 10% polyvinyl alcohol (PVA) is mixed into the pre-processed powder as a binder and ground to form uniform pellets. Then, the pellets were pressed under10 kPa into a cylinder (diameter = 12 mm, thickness = 6 mm). Finally, the raw cylinder were sintered at 1250–1350 °C, and heat preservation in the air for 4 h.

The phase composition was detected via the X-ray diffraction excited by Cu-Kα radiation source (XRD: Philips X'pert Pro MPD). The crystallographic parameters were obtained by refining the XRD data using the GSAS software. The Raman microscope (In Via, UK) with helium-neon laser source (i = 532 nm) was adopted to detect the lattice vibration spectrum in the range of 100–1100 cm^{-1}. The microstructure of the doped samples was observed via Scanning Electron Microscope (SEM: JEOL JSM-6490, Tokyo, Japan). Based on the Hakki-Coleman dielectric resonator method, the microwave dielectric properties of the sintered samples were measured using a vector network analyzer (Agilent N5230A, Agilent Technologies, USA) [21]. The temperature coefficient of resonant frequency value (TCF, τ_f) can be obtained by calculating the resonant frequency at different temperatures using the following equation:

$$\tau_f = \frac{f_{80} - f_{20}}{(T_{80} - T_{20}) \times f_{20}} \times 10^6 ppm \Big/ {}^{\circ}C \quad (1)$$

where f_{80} and f_{20} represent the resonant frequencies at 80 °C and 20 °C, respectively. The apparent density was measured by the Archimedes drainage method. The relative density (ρ_{re}) is the ratio of the measured density to the theoretical density (ρ_{th}), which is used to calculate the relative density, could be calculated by the follow equation.

$$\rho_{th} = \frac{MZ}{N_A V_C} \quad (2)$$

where, M, Z, N_A, and V_C represent the molar mass, the number of formula units per unit cell, the Avogadro's number, and the volume of a unit cell, respectively.

3. Results and discussion

The XRD patterns of the $Mg_{(1-x)}Ni_xTa_2O_6$ ceramics sintered at 1325 °C with different doping amounts are shown in Fig. 1. According to the standard $MgTa_2O_6$ structure (JSPDS # 84–1679), the crystallographic planes of the measured patterns were indexed, and no additional peaks were found, indicating that the Ni^{2+} successfully entered the crystal lattice and replaced Mg^{2+} to form a pure trirutile structure solid solution.

The detailed lattice parameters obtained via the Rietveld refinement method were shown in Fig. 2 and listed in Table 1. The measured patterns are consistent with the calculated data, which confirms that only a

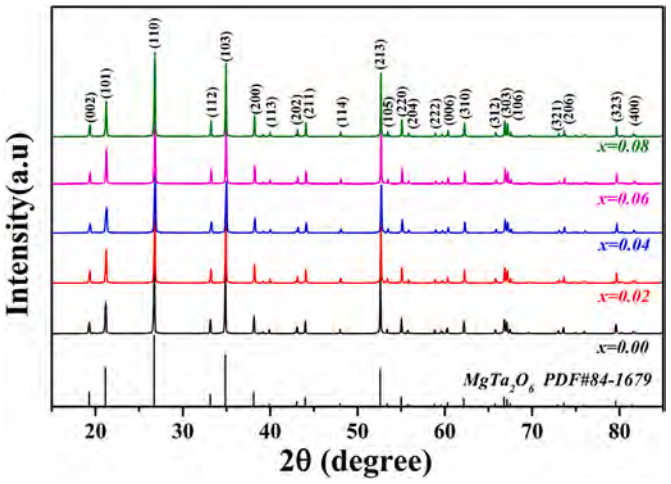

Fig. 1. XRD patterns of $Mg_{(1-x)}Ni_xTa_2O_6$ ceramics sintered at 1325 °C with different x content.

single-phase of trirutile structure existed in all doped samples. The reliability factor of R_p and R_{wp} are below 7% and 5%, respectively, which ensures the reliability of the refinement results. Furthermore, the cell parameters decrease with the addition of Ni^{2+}. This phenomenon is mainly caused by Ni^{2+} with a smaller ion radius(0.69 Å) entering the lattice instead of Mg^{2+} (0.72 Å) [22]. A schematic diagram of the trirutile structure is shown in Fig. 2(f). Mg^{2+} and Ta^{5+} occupy 2a and 4e Wyckoff positions, respectively, and form MgO_6 and TaO_6 octahedron with two adjacent O1 and four adjacent O2. Each MgO_6 octahedron binds to two-coordinated TaO_6 via a shared anion.

The Raman scattering spectrum is a valuable way to reflect the microstructure, phase transition, cation distributions, and defects of the solids by detecting bond vibrational characteristics. Based on group theory analysis, the character table of irreducible representations of the trirutile $MgTa_2O_6$ with space group $P4_2/mnm$ and point group D_{4h} are listed in Table 2. The irreducible representation of crystal vibrations modes is as follows [23].

$$\Gamma = 4A_{1g} + 2A_{2g} + 2B_{1g} + 4B_{2g} + 6E_g + A_{1u} + 4A_{2u} + 5B_{1u} + B_{2u} + 8E_u \quad (3)$$

The contribution of each atom at specific Wyckoff positions to the optical vibrational modes are listed in Table .3. Visibly, the A_{1g}, B_{1g}, B_{2g}, and E_g modes belong to Raman-active vibrations, while the E_u, A_{2u} are infrared-active vibrations. Compared with the undoped and previously reported spectra in Fig. 3(a) [24,25], there are no obvious hetero-peaks in the Raman spectrum of the doped samples, indicating that the doping amount within the experimental range does not cause distortion of crystal structure and phase composition. The proposed assignment of doped $MgTa_2O_6$ ceramics are listed in Table 4, and the deconvolved and fitted Raman spectra of x = 0.06 samples were given in Fig. 3(b). Because of the overlap of the Raman peaks and the measurement accuracy of the instrument, only 12 apparent Raman peaks can be distinguished between 100 and 1000 cm^{-1}. The most prominent peak (approximately 703.3 cm^{-1}) was assigned to the A_{1g} mode, which contributed to the symmetric Ta–O bond stretching vibration of the TaO_6 octahedron. Therefore, this vibration mode can deduce the structural information of oxygen octahedron, reflecting many physical characteristics [26,27].

The surface microstructure of different doped $Mg_{(1-x)}Ni_xTa_2O_6$ ceramics sintered at 1325 °C is exhibited in Fig. 4. Distinct grain boundaries and homogeneous micromorphology can be observed in all doped samples. The excellent consistency in the grain morphology and the absence of abnormal grains show that the introduction of an appropriate amount of Ni^{2+} does not lead to the abnormal growth of grains and the

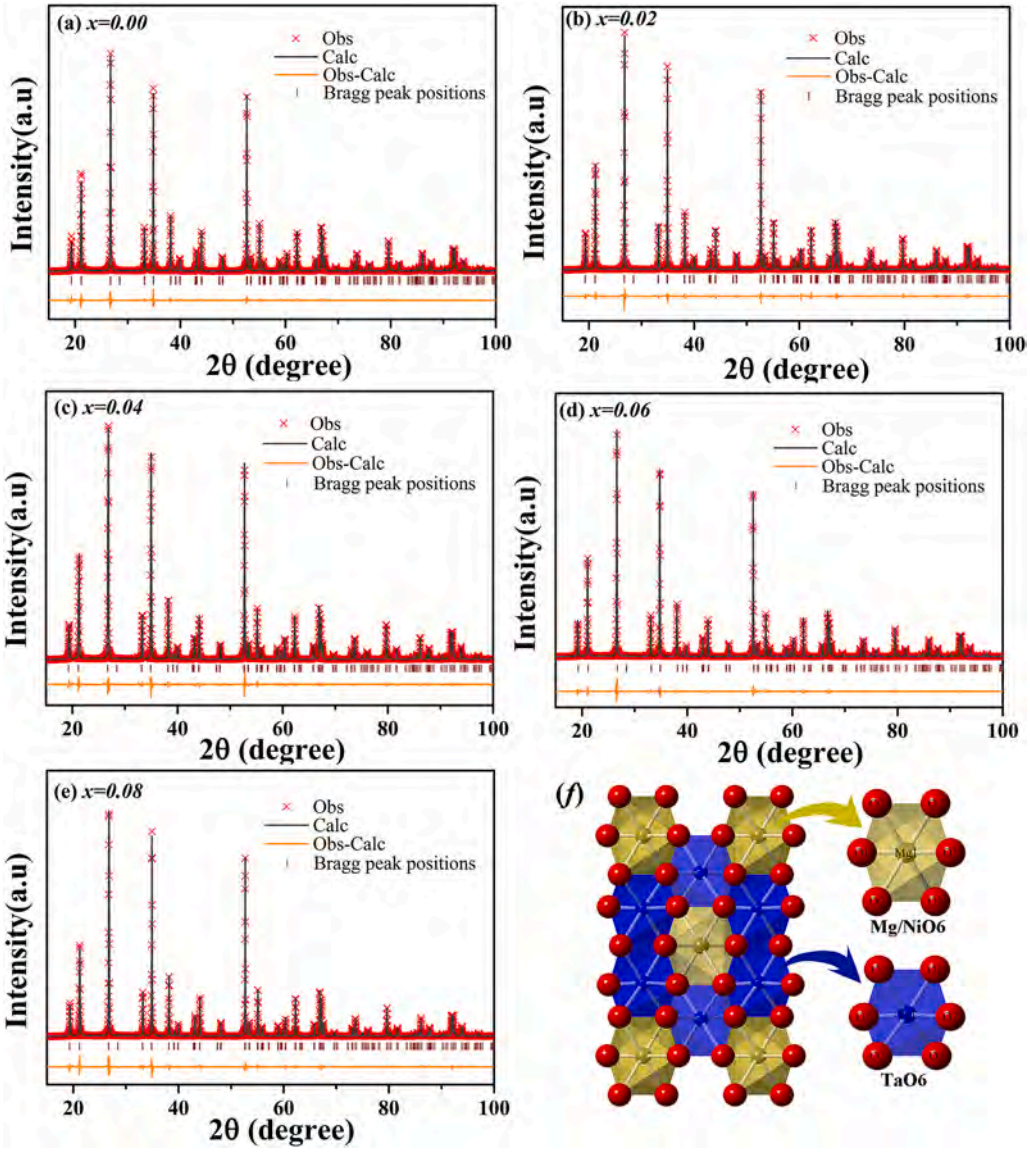

Fig. 2. Rietveld refinement patterns of $Mg_{(1-x)}Ni_xTa_2O_6$ ceramics sintered at 1325 °C with the different x content, and the crystal structure of $MgTa_2O_6$.

Table 1
The crystallographic parameters of the $Mg_{(1-x)}Ni_xTa_2O_6$ ceramics sintered at 1325 °C form the XRD refinement.(d: bond length).

Parameters	Doping				
	x = 0.00	x = 0.02	x = 0.04	x = 0.06	x = 0.08
a = b(Å)	4.7191	4.7190	4.7188	4.7108	4.7178
c (Å)	9.2129	9.2104	9.2087	9.2061	9.2037
V (Å^3)	205.172	205.107	205.050	204.930	204.857
d(Ta–O1)	1.8923	1.9084	1.9141	1.9200	2.0087
d(Ta–O2)	1.9993	2.0077	2.0111	1.8480	1.9833
d(Ta–O2)'	1.9423	1.9119	1.9300	2.0380	1.9665
d(Mg–O1)	2.2356	2.2122	2.1996	2.2445	2.0550
d(Mg–O2)	2.1336	2.1574	2.1311	2.1903	2.1186
R_{wp}(%)	6.19	5.52	6.29	6.72	6.73
R_p(%)	4.05	4.09	4.50	4.54	4.24

formation of heterogeneous phases.

The statistical grain distribution and calculated average grain size are shown in Fig. 5. The Ni^{2+} doping had a positive effect on grain growth. Previous studies showed that the quantity of grain boundaries, as a two-dimensional defect, is correspondingly reduced, which has a negative effect on the physical properties of the material [28,29]. Energy dispersive spectroscopy (EDS) of surface scanning was obtained to analyze the distribution of elements and the results are shown in Fig. 4 (f). According to the scanning results, the atomic number ratio of Mg, Ta, O, and Ni elements is consistent with the original chemical formula.

The relative density (ρ_{re}) of the doped samples sintered at different sintering temperatures are shown in Fig. 6. During heating, the unceasing growth of grains and grain boundaries eliminates pores and reduces defects, resulting in an increase in the relative density with increasing temperature. Upon further increasing the sintering temperature, the relative density decreased, which may be due to the poor sinterability at high temperature [16], resulting in some unexpected pores. Besides, at 1325 °C, the relative density of the various doped samples reached the optimum value with little fluctuation, indicating that doping within the experimental range does not seriously affect the micromorphology of $MgTa_2O_6$ ceramics.

Fig. 7 shows the variation in the permittivity with the sintering temperature and doping amount. The change of permittivity tends to increase markedly with temperature, which was due to the further densification of the microstructure with increasing temperature. In addition, after the temperature rose above 1325 °C, the dielectric

Table 2
Character table of irreducible representations.

modes	E	$2C_4$	C_2^z	$2C_2$	$2C_2'$	I	$2S_4$	σ_h	$2\sigma_v$	$2\sigma_d$	functions
A_{1g}	1	1	1	1	1	1	1	1	1	1	x^2+y^2,z^2
A_{2g}	1	1	1	−1	−1	1	1	1	−1	−1	J_z
B_{1g}	1	1	−1	1	−1	1	1	−1	1	−1	x^2-y^2
B_{2g}	1	1	−1	−1	1	1	1	−1	−1	1	xy
E_g	2	−2	0	0	0	2	−2	0	0	0	(xz,yz),(J_x,J_y)
A_{1u}	1	1	1	1	1	−1	−1	1	1	1	
A_{2u}	1	1	1	−1	−1	−1	−1	1	−1	−1	z
B_{1u}	1	1	−1	1	−1	−1	−1	−1	1	−1	
B_{2u}	1	1	−1	−1	1	−1	−1	−1	−1	1	
E_u	2	−2	0	0	0	−2	2	0	0	0	(x,y)

Table 3
Raman and IR Vibrational Modes of the $MgTa_2O_6$ structure.

Atom	Wyckoff position	x	y	z	Irreducible vibrational representations
Mg	2a	0	0	0	$A_{2u} + B_{1u}+2E_u$
Ta	4e	0	0	0.3319	$A_{1g} + A_{2u} + B_{1u} + B_{2g}+2E_u+2E_g$
O1	4f	0.3080	0.3080	0	$A_{1g} + A_{2g} + A_{2u} + B_{1g} + B_{1u} + B_{2g}+2E_u + E_g$
O2	8j	0.2970	0.2970	0.3230	$2A_{1g} + A_{2g} + A_{1u}+2A_{2u} + B_{1g}+2B_{1u}+ 2B_{2g} + B_{2u}+3E_u+3E_g$

$\Gamma_{Raman} = 4A_{1g}+2B_{1g}+4B_{2g}+6E_g$
$\Gamma_{IR} = A_{2u} + E_u$

Table 4
Deconvoluted Raman vibrational peak of doped $MgTa_2O_6$ structure.

modes	x = 0.00	x = 0.02	x = 0.04	x = 0.06	x = 0.08
B_{1g}	114.40	114.10	113.82	114.04	114.11
E_g	130.9	130.75	130.4	130.72	130.86
E_g	177.63	176.54	176.64	176.54	176.51
B_{2g}	207.52	207.05	206.46	206.64	206.68
A_{1g}	245.07	243.75	243.89	243.59	243.41
E_g	327.84	326.93	327.13	327.06	327.07
E_g	416.47	415.75	415.58	415.51	415.58
A_{1g}	465.47	465.58	465.6	465.71	465.83
E_g	504.74	504.83	504.74	503.85	504.02
B_{2g}	554.18	554.08	555.75	554.10	553.21
E_g	642.77	642.35	642.67	642.72	642.57
A_{1g}	704.74	703.46	703.37	703.26	703.13

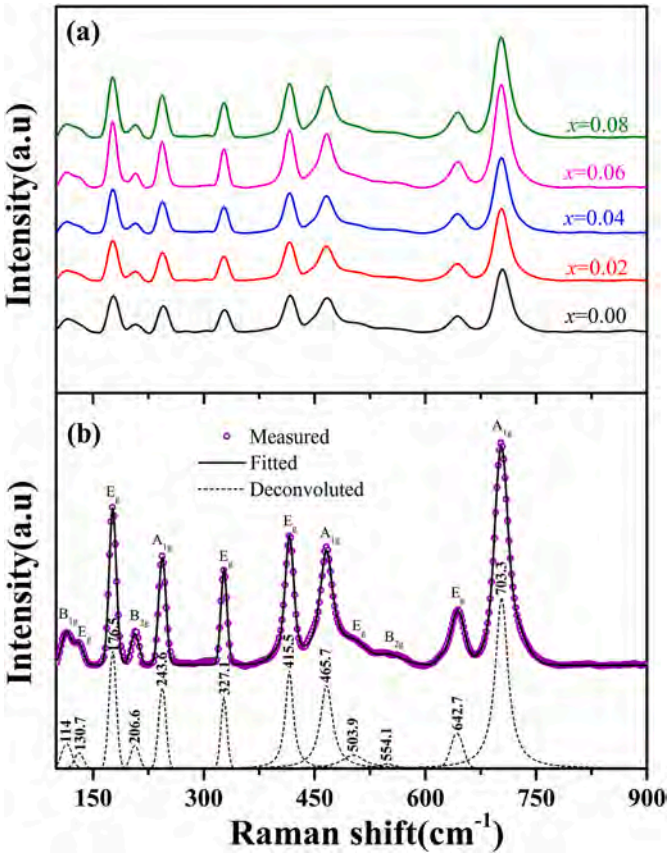

Fig. 3. The Raman spectra of doped $MgTa_2O_6$ ceramics (a) and the Deconvoluted Raman vibrational peak of x = 0.06 sample (b).

constant reaches a stable saturation value. Notably, with the increase of Ni^{2+} content, the measured dielectric constant decreased.

Pores are widely considered to be a critical external factor affecting the dielectric constant. Therefore, to study the internal factors effect on the dielectric, the following formula was used to calculate the pore-modified dielectric constant to eliminate the influence of compactness given that the dielectric constant remains unaffected by the porosity [30,31].

$$\varepsilon_m = \varepsilon_{mv}\left[1 - \frac{3p(\varepsilon_{mv}-1)}{2\varepsilon_{mv}+1}\right] \tag{4}$$

where ε_m, ε_{mv}, and p represent the measured permittivity, the corrected value of permittivity, and the porosity fraction (1-ρ_{re}), respectively. The modified value is greater than the measured value and shows a downward trend similar to the measured value, as shown in Fig. 8. Therefore, the introduction of Ni^{2+} inevitably causes internal changes, which lead to the variation of permittivity. Based on the chemical bond theory (PVL theory), the bond ionicity (f_i), caused by the mutual polarization between ions, contributes to the permittivity [32,33].

$$\varepsilon_r = \frac{n^2-1}{1-f_i} + 1 \tag{5}$$

where n represents the refractive index. To calculate the parameters such as bond ionicity via PVL theory, the complex crystal structure of $MgTa_2O_6$ needs to be decomposed into the sum of the diatomic expressions A_mB_n (A is cation and B is anion) [32,34].

$$\begin{aligned} MgTa_2O_6 &= MgTa_2O(1)_2O(2)_4 \\ &= Mg_{1/3}O(1)_{2/3} + Mg_{2/3}O(2)_{4/3} + Ta_{2/3}O(1)_{4/3} + Ta_{4/3}O(2)_{8/3} \end{aligned} \tag{6}$$

The bond ionicity of u chemical bond can be calculated by the following equations:

$$f_i^u = \frac{(C^u)^2}{(E_h^u)^2 + (C^u)^2} \tag{7}$$

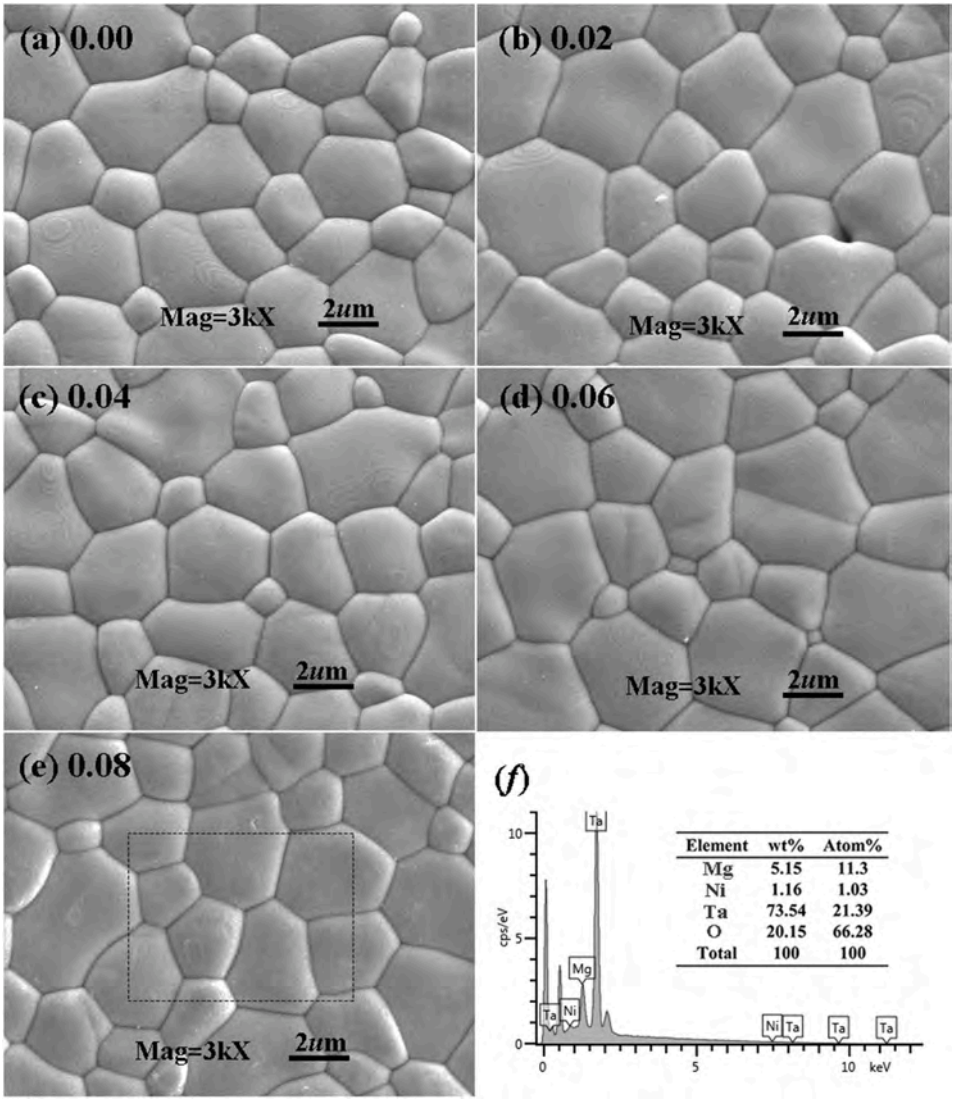

Fig. 4. The SEM images of $Mg_{(1-x)}Ni_xTa_2O_6$ ceramics sintered at 1325 °C with different x content (a–e), and the EDS results of x = 0.08 sample (f).

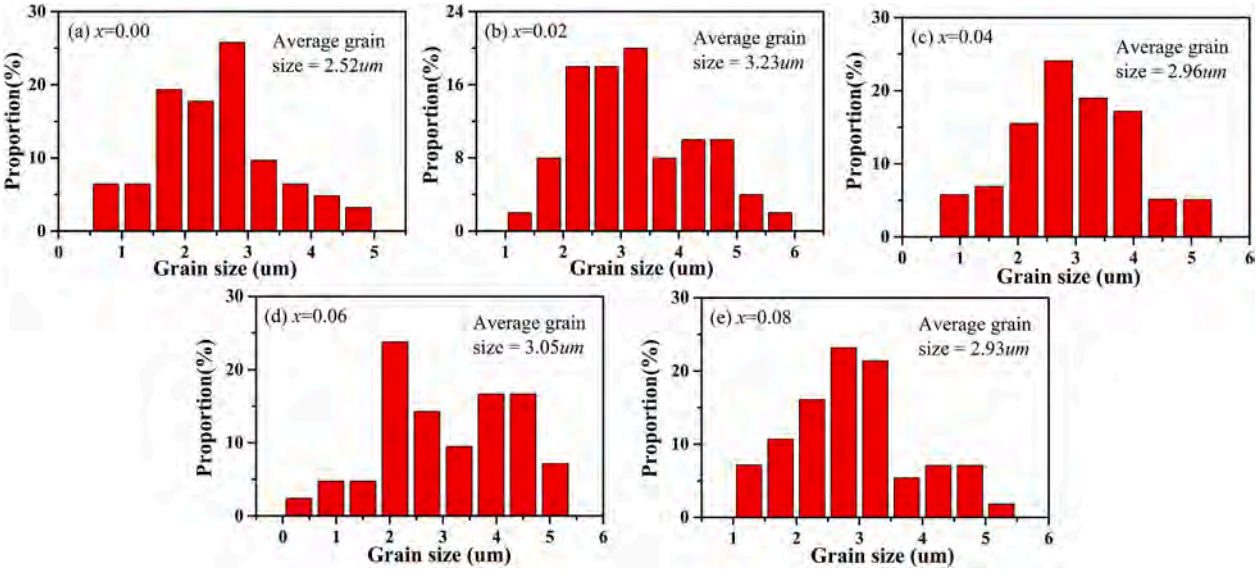

Fig. 5. The statistical grain distribution and calculated average grain size of $Mg_{(1-x)}Ni_xTa_2O_6$.

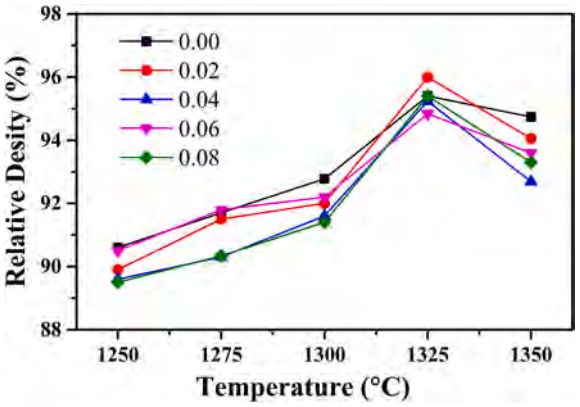

Fig. 6. The relative density of $Mg_{(1-x)}Ni_xTa_2O_6$ ceramics sintered at different temperature.

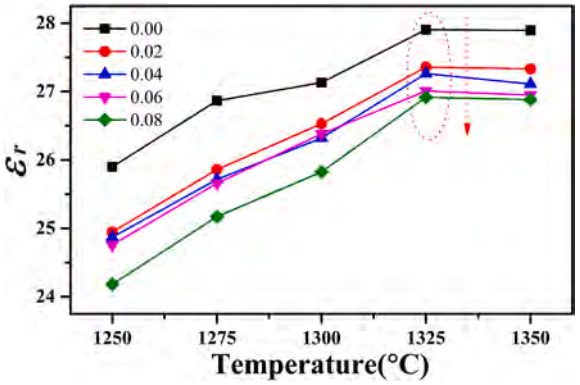

Fig. 7. The dielectric constant of $Mg_{(1-x)}Ni_xTa_2O_6$ ceramics.

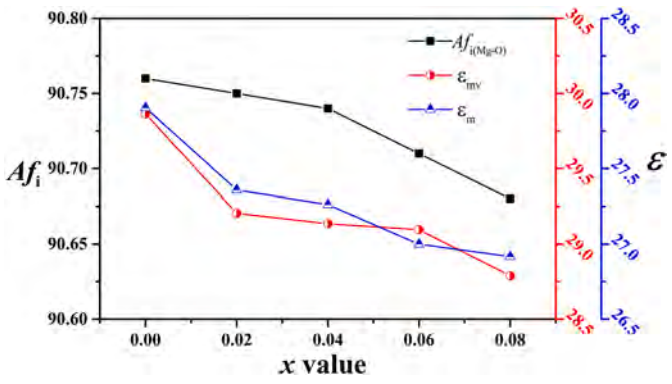

Fig. 8. The variation of average Mg–O bond ionicity (Af_i), the modified permittivity, and the measured permittivity of $Mg_{(1-x)}Ni_xTa_2O_6$ ceramics sintered at 1325 °C.

$$C^u = 14.4b^u \exp\left(-k_s^u r_0^u\right)\left[\left(Z_A^u\right)^* - \frac{n}{m}\left(Z_B^u\right)^*\right]\left(\frac{d^u}{2}\right)^{-1} \tag{8}$$

$$E_h^u = \frac{39.74}{\left(d^u\right)^{2.48}} \tag{9}$$

where E_h^u, C^u represent the homopolar part and heteropolar part of the energy gap.b^u represent a correction factor. $exp(-k_s^u r_0^u)$ is the Thomas-Fermi screening factor, could be obtained from the crystal structural parameters [33], and d^u is the bond length. $(Z_A^u)^*$ and $(Z_B^u)^*$ represent the effective number of valence electrons of A and B, respectively. The results of the average Mg–O bond ionicity (Af_i) are illustrated in Fig. 8. Significantly, the Mg–O bond ionicity decrease with the x value, reflecting the weakening of ion polarization, which results in a decrease in dielectric constant.

Fig. 9 shows the variation in the Q × f values with the sintering temperature and doping amount. During the initial heating process, the Q × f value increased uninterruptedly, which is similar to the change in the dielectric and density and was caused by the densification of the microstructure. However, the Q × f values appear to decrease substantially at excessive sintering temperature, which may be due to the poor sinterability. In addition, doping with Ni^{2+} was significantly enhanced the Q × f values compared with those of the undoped samples. The peak Q × f values were obtained for the ceramics sintered at 1325 °C, which increased to the optimal value of 173000 GHz (at 7.43 GHz) as the doping amount increased to 0.06. As the doping amount increased further, the Q × f value decreased. Based on the relative density and the XRD results of the samples sintered at 1325 °C, the relative density fluctuates in a small range without impurities phase. Therefore, the density and phase composition as an essential external factor could be neglected. Therefore, the density and phase composition, as essential factor affecting the Q × f values, could be ignored [27,35]. Crystal structural characteristics, which can be evaluated by the packing fraction (PF) and the lattice energy, are widely considered to be closely related to microwave dielectric properties [36]. The PF value could be obtained from the follow equation:

$$PF = \frac{volumeofpackedions}{volumeofunitcell} \times Z \tag{10}$$

where Z is 2 for $MgTa_2O_6$ structure. The calculated PF value is listed in Table 5. With the increase of Ni^{2+}, the PF values increase, which is a significant factor for the increase of Q × f values. According to the chemical bond theory, the lattice energy (U) represents the energy required for the decomposition of a compound. It reflects the stability of the crystal structure and is widely recognized to be closely related to the dielectric loss.

$$U = \sum_u U^u \tag{11}$$

$$U^u = U_c^u + U_i^u \tag{12}$$

$$U_c^u = 2100m\frac{\left(Z_+^u\right)^{1.64}}{\left(d^u\right)^{0.75}f_c^u} \tag{13}$$

$$U_i^u = 1270\frac{(m+n)Z_+^u Z_-^u}{d^u}\left(1 - \frac{0.4}{d^u}\right)f_i^u \tag{14}$$

where U_c^u, U_i^u represent the covalent part and the ionic part of the lattice energy, Z_+^u and Z_-^u is the valence state of A and B ions. The calculated

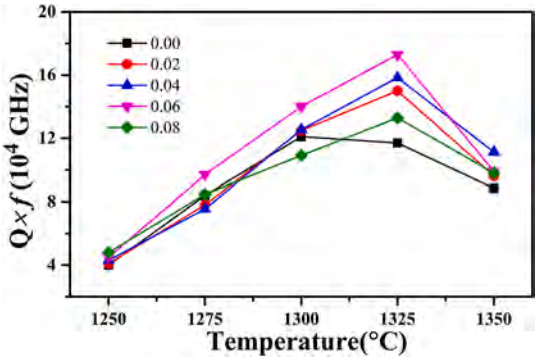

Fig. 9. The Q × f values of $Mg_{(1-x)}Ni_xTa_2O_6$ ceramics sintered at different temperature within x content.

Table 5
The lattice energy (*U*), FWHM values of A_{1g} mode (703 cm^{-1}), the Q × f values, the *TCF* values, and the bond energy of $Mg_{(1-x)}Ni_xTa_2O_6$ ceramics sintered at 1325 °C.

x	Q × f (10^4GHz)	U (10^3 kJ/mol)	FWHM	PF (%)	TCF (ppm/°C)
0	11.72	132.697	10.4575	70.89	34.7
0.02	15.12	132.779	10.4510	70.91	35.8
0.04	15.84	132.901	10.3477	70.93	34.4
0.06	17.30	133.011	10.3012	70.96	35.7
0.08	13.29	132.010	10.4120	70.99	35.4

results are summarized in Table 5. As the doping amount increases to 0.06, the lattice energy, and the Q × f values increases gradually. Further increasing the Ni^{2+} content caused both the lattice energy and Q × f values to decreased. According to the chemical bond theory, doping with Ni^{2+} improves the stability of $MgTa_2O_6$ ceramics to a certain extent, resulting in a decrease in the dielectric loss. Additionally, the full width at half maximum (FWHM) values are related to phonon lifetime, that is, a low FWHM value indicates highly bond-rigid oxygen-cage structures. Therefore, low FWHM values represent the longer decay of microwave energy propagation, resulting in higher Q × f values. Therefore, at excessive temperature, the increase of dielectric loss is mainly caused by a variety of internal factors [37], such as lattice energy and phonon lifetime.

The temperature coefficient of the resonance frequency (TCF) is another critical parameter of GHz application frequency, which characterizes the operating thermal stability at high frequency. The measured TCF values are listed in Table 5. The TCF values fluctuate slightly around 35 with the change of the doping amount, indicating that the introduction of Ni^{2+} will have an insignificant impact on the thermal stability of the resonant frequency of $MgTa_2O_6$ ceramics.

4. Conclusion

In this work, $Mg_{(1-x)}Ni_xTa_2O_6$ (x = 0, 0.02, 0.04, 0.06, 0.08) dielectric ceramics with a pure trirutile structure and dense morphology were synthesized. Analysis of the results substantiates that the introduction of Ni^{2+} does affect the crystal structure, which leads to an improvement of the microwave dielectric properties. According to the chemical bond theory calculation, the substitution of Ni^{2+} decreases the Mg–O bond ionicity, which affect the dielectric constant. Meanwhile, doping with Ni^{2+} increases the packing fraction and lattice energy, which improved the stability of the crystal structure and is beneficial to enhancing the microwave dielectric properties. However, the introduction of Ni^{2+} have an insignificant impact on the thermal stability of the resonant frequency of $MgTa_2O_6$ ceramics. Typically, an improved ceramic with satisfactory microwave dielectric properties: $\varepsilon_r = 27$, Q × f = 173,000 GHz (at 7.43 GHz), and $\tau_f = 35$ ppm/°C was synthesized.

Declaration of competing interest

The authors declare that they have no known competing financial interests or personal relationships that could have appeared to influence the work reported in this paper.

Acknowledgments

The National Natural Science Foundation of China (No. 51672036), the National Key Scientific Instrument and Equipment Development Project (No.51827802), Sichuan Science and Technology Program (No. 2020YFG0108) funded this work.

References

[1] H.W. Chen, H. Su, H.W. Zhang, T.C. Zhou, B.W. Zhang, J.F. Zhang, X.L. Tang, Low-temperature sintering and microwave dielectric properties of $(Zn_{1-x}Co_x)_2SiO_4$ ceramics, Ceram. Int. 40 (9) (2014) 14655–14659.
[2] S.E. Kalathil, U.A. Neelakantan, R. Ratheesh, Microwave dielectric properties of ultralow-temperature cofirable Ba3V4O13 ceramics, J. Am. Ceram. Soc. 97 (5) (2014) 1530–1533.
[3] C. Liu, L. Shi, Y. Lai, Y. Li, L. Jia, H. Su, J. Li, T. Wen, W. Ling, H. Zhang, B-site modification of $(Ba_{0.6}Sr_{0.4})TiO_3$ ceramics with enhanced diffuse phase transition behavior, Ceram. Int. 44 (7) (2018) 8109–8115.
[4] S. Lei, H. Fan, W. Chen, Effects of $CaO–B_2O_3$ glass addition on the low-temperature sintering and cation ordering in $Sr_xLa_{(1-x)}Ti_xAl_{(1-x)}O_3$ ceramics, J. Alloys Compd. 632 (2015) 78–86.
[5] A. Pashkin, S. Kamba, M. Berta, J. Petzelt, G.D.C.C.d. Györgyfalva, H. Zheng, H. Bagshaw, I.M. Reaney, High frequency dielectric properties of $CaTiO_3$-based microwave ceramics, J. Phys. D Appl. Phys. 38 (5) (2005) 741–748.
[6] P. Wang, Y.R. Wang, J.X. Bi, H.T. Wu, Effects of Zn^{2+} substitution on the crystal structure, Raman spectra, bond energy and microwave dielectric properties of Li_2MgTiO_4 ceramics, J. Alloys Compd. 721 (2017) 143–148.
[7] T. Tsunooka, M. Androu, Y. Higashida, H. Sugiura, H. Ohsato, Effects of TiO_2 on sinterability and dielectric properties of high-Q forsterite ceramics, J. Eur. Ceram. Soc. 23 (14) (2003) 2573–2578.
[8] Y. Guo, H. Ohsato, K.-i. Kakimoto, Characterization and dielectric behavior of willemite and TiO_2-doped willemite ceramics at millimeter-wave frequency, J. Eur. Ceram. Soc. 26 (10–11) (2006) 1827–1830.
[9] Q. Lin, K. Song, B. Liu, H.B. Bafrooei, D. Zhou, W. Su, F. Shi, D. Wang, H. Lin, I. M. Reaney, Vibrational spectroscopy and microwave dielectric properties of $AY_2Si_3O_{10}$ (A=Sr, Ba) ceramics for 5G applications, Ceram. Int. 46 (1) (2020) 1171–1177.
[10] D. Zhou, L.-X. Pang, D.-W. Wang, I.M. Reaney, $BiVO_4$ based high k microwave dielectric materials: a review, J. Mater. Chem. C 6 (35) (2018) 9290–9313.
[11] H.H. Guo, D. Zhou, W.F. Liu, L.X. Pang, D.W. Wang, J.Z. Su, Z.M. Qi, Microwave dielectric properties of temperature-stable zircon-type (Bi, Ce)VO_4 solid solution ceramics, J. Am. Ceram. Soc. 103 (1) (2019) 423–431.
[12] D. Zhou, L.-X. Pang, D.-W. Wang, H.-H. Guo, F. Yang, Z.-M. Qi, C. Li, B.-B. Jin, I. M. Reaney, Crystal structure, impedance and broadband dielectric spectra of ordered scheelite-structured $Bi(Sc_{1/3}Mo_{2/3})O_4$ ceramic, J. Eur. Ceram. Soc. 38 (4) (2018) 1556–1561.
[13] Hyo-Jong Lee, I.-T. K, a.K.S. Hong, Dielectric properties of AB_2O_6 compounds at microwave frequencies (A=Ca, Mg, Mn, Co, Ni, Zn,and B=Nb, Ta), J. Appl. Phys. 36 (1997) 1318–1320.
[14] M. Dang, H. Ren, X. Yao, H. Peng, T. Xie, H. Lin, L. Luo, Investigation of phase composition and microwave dielectric properties of MgO-Ta_2O_5 ceramics with ultrahigh Qf value, J. Am. Ceram. Soc. 101 (7) (2018) 3026–3031.
[15] W.-C. Tzou, Y.-C. Chen, C.-F. Yang, C.-M. Cheng, Microwave dielectric characteristics of $Mg(Ta_{1-x}Nb_x)_2O_6$ ceramics, Mater. Res. Bull. 41 (7) (2006) 1357–1363.
[16] E.S. Kim, S.J. Kim, Effect of sintering temperature on the microwave dielectric properties of MgB_2O_6(B = Nb^{5+}, Ta^{5+}) ceramics, Ferroelectrics 388 (1) (2009) 93–100.
[17] H.-J. Lee, K.-S. Hong, I.-T. Kim, Crystal structure and microwave dielectric properties of $M(Nb_xTa_{1-x})_2O_6$ solid solution (M=Mg or Zn), J. Mater. Res. 12 (6) (2011) 1437–1440.
[18] Y. Zhang, Z. Yue, X. Qi, B. Li, Z. Gui, L. Li, Microwave dielectric properties of Zn $(Nb_{1-x}Ta_x)_2O_6$ ceramics, Mater. Lett. 58 (7–8) (2004) 1392–1395.
[19] C.-L. Huang, W.-R. Yang, P.-C. Yu, High-Q microwave dielectrics in low-temperature sintered $(Zn_{1-x}Ni_x)_3Nb_2O_8$ ceramics, J. Eur. Ceram. Soc. 34 (2) (2014) 277–284.
[20] W. Yang, C. Pan, C. Huang, Influence of Mg substitutions for Zn on the phase relation and microwave dielectric properties of $(Zn_{1-x}Mg_x)_3Nb_2O_8$ (x=0.02–1.0) system, J. Alloy. Comp. 581 (2013) 257–262.
[21] B.W. Hakki, P.D. Coleman, A dielectric resonator method of measuring inductive capacities in the millimeter range, IRE Trans. Microwave Theory Techn. 8 (4) (1960) 402–410.
[22] G. Wang, H. Zhang, F. Xu, X. Huang, Y. Lai, G. Gan, Y. Yang, J. Li, C. Liu, L. Jin, Investigation and characterization on crystal structure and enhanced microwave dielectric properties of non-stoichiometric $Li_{3+x}Mg_2NbO_6$ ceramics, Ceram. Int. 44 (16) (2018) 20539–20544.
[23] S. Jia, Q. Zhou, F. Huang, F. Li, Y. Hu, L. Huang, L. Li, Y. Li, T. Cui, High-pressure Raman scattering and x-ray diffraction studies of MgTa2O6, AIP Adv. 10 (6) (2020).
[24] H. Haeuseler, Infrared and Raman spectra and normal coordinate calculations on trirutile-type compounds, Spectrochim. Acta Mol. Spectros 37 (7) (1981) 8.
[25] D. Xu, S. Gao, W. Liu, Y. Liu, Q. Zhou, L. Li, T. Cui, H. Yuan, The Raman scattering of trirutile structure MgTa2O6 single crystals grown by the optical floating zone method, RSC Adv. 9 (2) (2019) 839–843.
[26] M.Y. Chen, C.T. Chia, I.N. Lin, L.J. Lin, C.W. Ahn, S. Nahm, Microwave properties of $Ba(Mg_{1/3}Ta_{2/3})O_3$, $Ba(Mg_{1/3}Nb_{2/3})O_3$ and $Ba(Co_{1/3}Nb_{2/3})O_3$ ceramics revealed by Raman scattering, J. Eur. Ceram. Soc. 26 (10–11) (2006) 1965–1968.
[27] Q. Liao, L. Li, Structural dependence of microwave dielectric properties of ixiolite structured $ZnTiNb_2O_8$ materials: crystal structure refinement and Raman spectra study, Dalton Trans. 41 (23) (2012) 6963–6969.
[28] N. Ichinose, T. Shimada, Effect of grain size and secondary phase on microwave dielectric properties of $Ba(Mg_{1/3}Ta_{2/3})O_3$ and $Ba([Mg,Zn]_{1/3}Ta_{2/3})O_3$ systems, J. Eur. Ceram. Soc. 26 (10–11) (2006) 1755–1759.

[29] G. Wang, D.N. Zhang, X. Huang, Y.H. Rao, Y. Yang, G.W. Gan, Y.M. Lai, F. Xu, J. Li, Y.L. Liao, C. Liu, L.C. Jin, V.G. Harris, H.W. Zhang, Crystal structure and enhanced microwave dielectric properties of Ta^{5+} substituted $Li_3Mg_2NbO_6$ ceramics, J. Am. Ceram. Soc. 103 (1) (2020) 214–223.

[30] S.J. Penn, N.M. Alford, A. Templeton, X.R. Wang, M.S. Xu, M. Reece, K. Schrapel, Effect of porosity and grain size on the microwave dielectric properties of sintered alumina, J. Am. Ceram. Soc. 80 (7) (1997) 1885–1888.

[31] L. Shi, C. Liu, H. Zhang, R. Peng, G. Wang, X. Shi, X. Wang, W. Wang, Crystal structure, Raman spectroscopy, metal compatibility and microwave dielectric properties of $Ce_2Zr_3(MoO_4)_9$ ceramics, Mater. Chem. Phys. 250 (2020) 7.

[32] B.F. Levine, Bond susceptibilities and ionicities in complex crystal structures, J. Chem. Phys. 59 (3) (1973) 1463–1486.

[33] P. Zhang, Y. Zhao, X. Wang, The relationship between bond ionicity, lattice energy, coefficient of thermal expansion and microwave dielectric properties of $Nd(Nb_{(1-x)}Sb_{(x)})O_4$ ceramics, Dalton Trans. 44 (24) (2015) 10932.

[34] H.L. Pan, L. Cheng, Y.X. Mao, H.T. Wu, Investigation and characterization on crystal structure of ixiolite structure ATiNb2O8 (A = Mg, Zn) ceramics at microwave frequency based on the complex chemical bond theory, J. Alloys Compd. 693 (2017) 792–798.

[35] J. Zhang, R. Zuo, A. Feteira, Effect of ordering on the microwave dielectric properties of spinel-structured $(Zn_{1-x}(Li_{2/3}Ti_{1/3})_x)_2TiO_4$ ceramics, J. Am. Ceram. Soc. 99 (10) (2016) 3343–3349.

[36] E.S. Kim, B.S. Chun, R. Freer, R.J. Cernik, Effects of packing fraction and bond valence on microwave dielectric properties of $A^{2+}B^{6+}O_4$ (A^{2+}: Ca, Pb, Ba; B^{6+}: Mo, W) ceramics, J. Eur. Ceram. Soc. 30 (7) (2010) 1731–1736.

[37] Y. Zhang, Y. Zhang, M. Xiang, Crystal structure and microwave dielectric characteristics of Zr-substituted $CoTiNb_2O_8$ ceramics, J. Eur. Ceram. Soc. 36 (8) (2016) 1945–1951.